Efficient Prediction of Aerodynamic Control Surface Responses using the Linear Frequency Domain

Ruben B. Seidler*, Sebastian Marten†, Markus Widhalm‡ and Jochen Wild§
DLR German Aerospace Center, Braunschweig, D-38108, Germany

In modern aircraft design the accurate prediction of dynamic control surface deflections is crucial for the evaluation and application of new load alleviation techniques. Time-marching approaches, such as the unsteady Reynolds-averaged Navier-Stokes equations, do provide a complete modeling of the aerodynamic flow field, however, they are extremely time-consuming and still too expensive for design applications. In this article a model is presented, which enables the fast and accurate prediction of aerodynamic responses for arbitrary control surface deflections. The model hereby reflects the time signal of the control surface deflection as a superposition of frequency components and computes the dynamic response behavior of the control surface using the linear frequency domain. The frequency responses are precomputed in a surrogate model for a wide parameter space of Mach number, Reynolds number, angle of attack and flap chord ratio, so that a frequency response for a new flight condition can be computed by mere interpolation. After building the surrogate model, the method achieves reduction in computational time of up to 6 orders of magnitude in comparison to time-marching simulations, while still covering the viscous and unsteady aerodynamic effects in the flow.

I. Nomenclature

A	=	amplitude of oscillation
c	=	chord length
c_L	=	section lift coefficient
f	=	frequency
$\hat{\mathbf{g}}$	=	frequency response
k	=	reduced frequency
l_{ref}	=	reference length
Ma	=	Mach number

*Research Engineer, Institute of Aerodynamics and Flow Technology, Transport Aircraft, ruben.seidler@dlr.de
†Research Engineer, Institute of Aerodynamics and Flow Technology, Transport Aircraft, sebastian.marten@dlr.de
‡Research Scientist, Institute of Aerodynamics and Flow Technology, CASE branch, markus.widhalm@dlr.de
§Research Scientist and Team Lead High-Lift, Institute of Aerodynamics and Flow Technology, Transport Aircraft, jochen.wild@dlr.de, Senior AIAA member

N = number of data points

$\mathbf{R}$ = residual

r = magnitude

Re = Real part operator

Re = Reynolds number

T = time period

t = time

U_∞ = freestream velocity

$\mathbf{u}$ = conservative state vector

$\mathbf{x}$ = grid node coordinates

$\dot{\mathbf{x}}$ = grid node velocities

c_f/c = flap chord ratio

α = angle of attack

δ_f = flap deflection angle

ω = angular frequency

ϕ = phase shift

II. Introduction

In modern aviation the possibilities given by the increasing computing capacity and by the capabilities of multifunctional control devices lead to a significantly more adaptive aircraft design. Especially the subject of load alleviation becomes more and more feasible in terms of computational power and applicability of the control surfaces on the wing. Load alleviation aims to reduce structural loads on the wing and decrease the necessary structural strength and thereby the weight of the wing. Initial studies of Xu and Kroo [1] indicated an reduction of up to 11% in fuel burn and 7% in direct operating costs for the simultaneous application of maneuver and gust load alleviation, which shows its strong potential for the improvement of new aircraft designs. One possibility for active load alleviation is the use of control surfaces on the wing to mitigate the effect of gust and maneuvers on the wing structure. For gusts, in particular, the flap reaction time and deflection speed needs to be fast, which causes the occurrence of unsteady aerodynamic effects in the flow. Furthermore, the necessary accurate gust and maneuver simulations must be computed for a wide range of flow conditions and wing geometries. Therefore, in interaction with time-dependent control surface deflections, the computational fluid dynamic (CFD) calculations for the aerodynamic responses require a high amount of computational resources and time. Unsteady Reynolds-averaged Navier-Stokes (URANS) simulations enable the complete modeling of the time-accurate results for the aerodynamic response behavior. However, despite the increasing computational

power and acceleration of numerical techniques, URANS computations are still too time-consuming and therefore too expensive for extensive industrial design applications.

The method presented in this article enables to determine the aerodynamic response coefficients for arbitrary flap deflections in real time. The time-accurate behavior of the control surface is thereby modeled as a superposition of frequency components in the frequency domain. It uses the computations of the well-established linear frequency domain (LFD) solver to efficiently compute the dynamic response behavior of the control surface. The dynamic response behavior is computed as the frequency response, which describes the magnitude and phase shift of the control surface for every frequency. Since the dynamic response behavior for all frequencies is represented in the frequency response, the method is able to predict the unsteady aerodynamic effects for fast and arbitrary flap deflections.

The implementation of linear frequency domain methods itself has found a broad area of application in the field of aeroelastic analysis using computational fluid dynamics. Initial practical applications of LFD methods have been the domain of turbomachines, where flow-structure interactions excite vibrations in the structural parts. Frequency domain methods are thereby commonly applied for the analysis of the effect of viscous, unsteady flows fields on the aeroelastic stability. Clark and Hall [2] used time-linearized Navier-Stokes analysis for the accurate simulation of unsteady aerodynamics of turbomachinery stall flutter. Hall et al. [3] validated the efficiency and accuracy of frequency domain approaches for complex and nonlinear flows inside of turbomachines for aeromechanic problems such as flutter and gust response. In their studies they also used harmonic balance methods, which in comparison to the LFD can also reflect nonlinear effects at higher amplitudes. Dufour et al. [4] used harmonic balance methods to correctly predict flow patterns for rotor and stator interactions, while drastically reducing the required simulation time.

Regarding the application of LFD methods on aircraft, a number of researchers used LFD methods on aircraft models for the efficient prediction of dynamic derivatives as a surrogate for URANS simulations. Widhalm et al. [5] evaluated dynamic derivatives over a wide parameter space for the computation of aerodynamic loads for a full aircraft configuration. Studies on time-linearized methods were done by Thormann and Widhalm [6][7] for the accurate prediction of pitch oscillations in viscous transonic flows and for shock-induced flow separation on a wing. By using the LFD method they could achieve time savings in comparison to URANS simulations of up to two orders of magnitude. While the time domain signal is a superposition of frequency components in the LFD, Ghoreyshi and Cummings [8] successfully modeled the time signal of a control surface deflection as a superpositon of impulses. They proved that the unsteady effects have a strong impact on amplitude and phase shifts of the airloads in comparison to steady-state predictions. Results by Da Ronch et al. [9] showed that the LFD method becomes inaccurate for strong dynamic nonlinearities, because it covers only the first harmonic in the frequency domain. For a higher accuracy in those cases the harmonic balance method with the computation of more harmonics is required. LFD methods presuppose that the considered system of equations behaves linear for high amplitudes and that it is linear time-invariant [7].

Here, the frequency responses of the LFD solver are used in a surrogate model, so that a frequency response for a new

flight condition can be computed efficiently by mere interpolation. Hence, the lift response in the surrogate model for arbitrary flight conditions and flap movements can be evaluated with greatly reduced computational costs. The applied surrogate model uses a response surface methodology (RSM), in which the inputs are a flap movement over a period of time and parameters for flight condition and geometric design.

The application of surrogate models allows the efficient and accurate simulation of unsteady aerodynamics and aeroelastic responses in the structure, while aiming to decrease the required computational costs and time. In previous studies surrogate models have been used for the efficient computation of the effect of purely aerodynamic or geometric variations on the flow field. Bekemeyer et al. [10][11] developed and examined a surrogate model for gust simulations on a 2D NACA0012 airfoil using computational fluid dynamics. In their model the aerodynamic responses for various sinusoidal gusts are determined using the linearized frequency domain. Thereby, the aerodynamics for arbitrary gusts can be efficiently solved with a superposition of the precomputed frequency components. Bekemeyer et al. [12] also successfully implemented the application of the linear frequency domain solver for a first basic gust controller on a 3D aircraft to simulate realistic gust-encounter scenarios. Motta and Quaranta [13] presented a reduced-order model (ROM) for the accurate simulation of the unsteady aerodynamics on an L-shaped gurney flap. In this model, the prediction of unsteady loads of the airfoil and the device are covered also by utilizing the advantages of the frequency domain. Glaz et al. [14] used a reduced order model approach for the prediction of unsteady aerodynamics on pitching/plunging motions of airfoils. They used a surrogate-based recurrence framework for the prediction of time domain solutions of aerodynamic forces and moments to reduce the computational costs significantly.

In this work the surrogate model is used in order to efficiently and accurately predict their dynamic lift response behavior for arbitrary control surface deflections. The response variable in this model is the lift coefficient response for the flap in the same period of time. The method is presented and applied on 2D wing sections of a transonic airfoil. The results for a plain flap and a Fowler flap are shown in order to verify the applicability of the methodology on different flap systems. The aerodynamic parameters Mach number, Reynolds number, and the angle of attack are varied. The variation of the flap chord size is an additional geometric parameter for the plain flap. Results for both flap systems are computed in subsonic flow regions with deflection angles up to 20°, whereas for the plain flap also results in transonic flow with deflection angles up to 2° are shown. URANS simulations serve for comparison in terms of accuracy and computational efficiency of the method. The present article is the latest and revised version of our article, presented at the AIAA Scitech 2019 Forum [15].

III. Description of the Core LFD Method

This section details the process on how to determine the aerodynamic response behavior for an arbitrary flap movement in a time period using the frequency domain for a specific flight condition and flap geometry. The basis for the core method in this work is the computation of the aerodynamic response of a time signal in the linear frequency

domain. This method provides the theoretical basis for the surrogate model and it is in itself a closed and functional process.

A. Model of the flap systems

The method is applied on two different flap systems. Models for the respective two types of flaps are shown in Fig. 1. The Fowler flap (a) is a common high-lift device, where the flap is separated from the primary airfoil and moves downward from the retracted starting position. Thus, it is capable of increasing chord and rotation angle of the flap. The Fowler flap used in this work has a fixed extension and is limited to rotation of the flap angle, because for initial testing of the method the frequency response for only one degree of freedom should be used, i.e. the rotation of the flap. The second system is a plain flap (b), which is defined through a rotation of a rear portion of the airfoil. The center of rotation (COR) is located at the leading edge of the flap, so that the junction between airfoil and flap needs to deform. The plain flap is characterized by its simplicity and relative to other systems it is less efficient in terms of impact on the lift. Nevertheless, the plain flap represents a more complex numerical application case, because the deforming section at the COR for high amplitudes and variable COR positions needs to be modeled and tested for the LFD. In the figure the

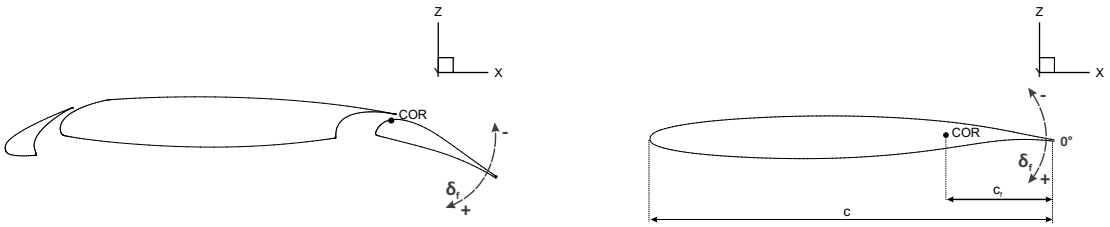

(a) fowler flap (b) plain flap

Fig. 1 Model of the Fowler flap and the plain flap movement.

sign for positive and negative deflections are marked. Additionally, for the plain flap the chord length c and the variable flap chord length c_f are depicted.

B. Transition to the frequency domain

The deflection angle over a defined time period is referred to as the flap movement profile $\delta_\mathrm{f}(t)$. For the transformation of the flap movement profile into the frequency domain $\delta_\mathrm{f}(i\omega)$ the fast Fourier transform (FFT) algorithm is used. The FFT is an algorithm for the fast computation of the discrete Fourier transform (DFT)[16]. For the FFT in this work there are two kinds of time series data: the flap movement profile $\delta_\mathrm{f}(t)$ and the lift coefficient response over time $c_L(t)$. As a first step, the flap movement profile $\delta_\mathrm{f}(t)$ is shifted into the frequency domain by:

$$\hat{\delta}_\mathrm{f}(i\omega_j) = \sum_{n=0}^{N-1} \delta_\mathrm{f}(t_n) e^{-i\omega_j t_n}, \qquad \omega_j = j\frac{2\pi}{N\Delta t}, \qquad t_n = n\Delta t, \qquad j = 0, 1, ..., N-1 \tag{1}$$

In this equation t_n is the time series value, Δt is the sampling time step and N is the resolution of the flap movement profile. Furthermore, $N\Delta t$ is the time period T of the flap movement profile and $2\pi/T$ is the smallest non-zero resolvable angular frequency ω_1. For a smaller non-zero resolvable frequency ω_1, the time period T needs to be increased, while for a higher maximum frequency $2\pi/\Delta t$, the time step Δt needs to be decreased.

In consequence, the discrete Fourier transform divides the flap movement profile into its frequency components. Every frequency component represents a sinusoidal curve with its own amplitude and phase shift depicting its component of the input signal. The sinusoidal curve in the time domain y for a given base frequency ω is described by:

$$y(\omega) = A(\omega)\sin(\omega t + \phi(\omega)) \tag{2}$$

In this equation A is the amplitude and ϕ is the phase shift of the signal.

A characteristic parameter for the analysis of unsteady flows is the reduced frequency k. It is a dimensionless quantity, which gives an indication for the unsteadiness of the flow field. The reduced frequency k is defined as:

$$k = \frac{\omega}{U_\infty}\frac{c}{2} \tag{3}$$

ω is hereby the angular frequency, c is the chord length and U_∞ is the freestream velocity. This parameter is important for the analysis of the flap response behavior in the frequency domain, because it indicates the occurrence of unsteady aerodynamics in the flow caused by the flap movement. Between $k = 0 - 0.05$ the flow is said to be quasi-steady [17], which means that the dynamic effects of the movement are too small and the flap has the same effectiveness as if it would be in a steady state. For $k > 0.2$ strong unsteady aerodynamic effects occur in the flow and heavily influence the pressure distribution of the airfoil and thereby the effectiveness of the flap.

In Fig. 2 three generic flap movement profiles with a time period of 5 seconds are shown in the time domain (a) and their counterpart in the frequency domain (b). These profiles are chosen to highlight the influence of different flap movements on the frequency domain.

In Fig. 2 (b) it can be seen that for all three profiles the largest components of the input signal are in the low frequency range below $k = 0.1$. This illustrates that for typical applications in aviation low frequencies have a dominant part on the impact on the aerodynamic response behavior of the flap. The profile b has the highest maximum flap rotation speed of 100 °/s and therefore, there are still frequency components of the input signal above $k = 0.5$. The influence of unsteady aerodynamics effects increases at higher flap movement speeds and the dynamic response behavior of the flap for higher frequency ranges needs to be considered.

It should be noted that in the frequency domain every frequency component apart from the amplitude also has a phase shift. The phase shifts for the flap movement profiles are not illustrated because they vary heavily with different profiles

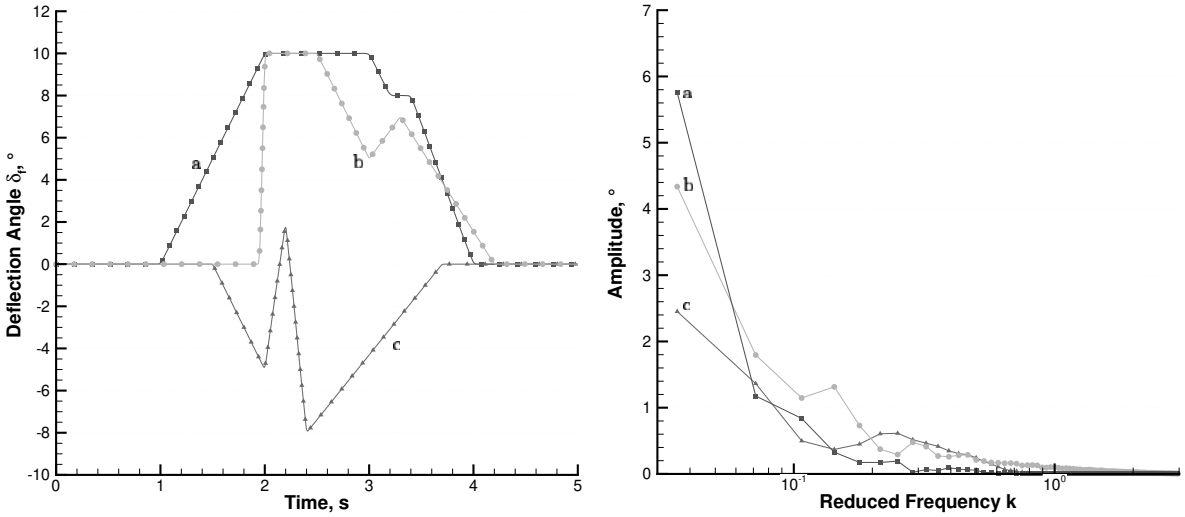

(a) time domain (b) frequency domain

Fig. 2 Three generic flap movement profiles in the time (a) and frequency domain (b).

and there is no additional value in analysing them in this section. After transferring the flap movement profile in the frequency domain, the method now requires the dynamic response behavior of the flap represented by the frequency response.

C. Computation of the frequency response using the LFD solver

The LFD solver is used to compute the frequency response of the flap. The required LFD solver is provided by the DLR TAU code [18] and calculates the first harmonic for small-disturbance solutions of the RANS equations. Therefore steady-state RANS solutions of the flow are required, which are also computed by the DLR TAU code. For the turbulence modeling the negative one-equation Spalart-Allmaras (SA-neg) model [19] was used in order to achieve a high convergence and robustness in the solution. The TAU LFD solver models unsteady motions as a superposition of the steady state and a perturbation[6]. Equation (4) describes the fluid motion discretized in space in a semi-discrete form:

$$\frac{\mathrm{d}\mathbf{u}(t)}{\mathrm{d}t} + \mathbf{R} = 0, \qquad \mathbf{R} := \mathbf{R}(\mathbf{u}(t), \mathbf{x}(t), \dot{\mathbf{x}}(t)) \tag{4}$$

Hereby, $\mathbf{R}$ is the residual and a function of the conservative state vector $\mathbf{u}$, the grid-node coordinates $\mathbf{x}$, and the grid node velocities $\dot{\mathbf{x}}$. The conservative state vector $\mathbf{u}$ contains the variables for the flow equations, specifically the mass, momentum, energy and the SA viscosity in the flow. Under the assumption that an unsteady periodic motion consists of a steady state and a small perturbation, the time-dependent variables $\mathbf{u}(t)$ and $\mathbf{x}(t)$ can be constructed as:

$$\mathbf{u}(t) = \overline{\mathbf{u}} + \tilde{\mathbf{u}}(t), \qquad \|\tilde{\mathbf{u}}\| << \|\overline{\mathbf{u}}\| \tag{5}$$

$$\mathbf{x}(t) = \overline{\mathbf{x}} + \tilde{\mathbf{x}}(t), \qquad \|\tilde{\mathbf{x}}\| << l_{ref} \tag{6}$$

The variable $\overline{\mathbf{u}}$ describes the steady-state time-invariant part, whereas $\tilde{\mathbf{u}}$ describes the time-dependent perturbation. The perturbation of the flow variables in the unsteady motion $\|\tilde{\mathbf{u}}\|$ is assumed to be significantly smaller than the steady-state value $\|\overline{\mathbf{u}}\|$. Equally, the perturbation of the grid node motion is significantly smaller than the reference length l_{ref}. The residual $\mathbf{R}$ is defined by:

$$\mathbf{R} \approx \overline{\mathbf{R}} + \frac{\partial \mathbf{R}}{\partial \mathbf{u}}\tilde{\mathbf{u}}(t) + \frac{\partial \mathbf{R}}{\partial \mathbf{x}}\tilde{\mathbf{x}}(t) + \frac{\partial \mathbf{R}}{\partial \dot{\mathbf{x}}}\tilde{\dot{\mathbf{x}}}(t), \qquad \overline{\mathbf{R}} := \mathbf{R}(\overline{\mathbf{u}}, \overline{\mathbf{x}}) \approx 0 \tag{7}$$

For a well converged steady-state solution the residual $\overline{\mathbf{R}}$ is close to zero and can be neglected. Since both, the motion of the grid nodes and the resulting flow solution are assumed to be periodic, the time-dependent perturbation part in equations (5) and (6) can be split into its frequency parts by a Fourier decomposition:

$$\tilde{\mathbf{u}}(t) = \sum_j \mathrm{Re}(\hat{\mathbf{u}}_j e^{i\omega_j t}) \tag{8}$$

$$\tilde{\mathbf{x}}(t) = \sum_j \mathrm{Re}(\hat{\mathbf{x}}_j e^{i\omega_j t}) \tag{9}$$

The variable Re represents the real part operator in the Fourier series and is dropped in the following equation for an improved readability. The variable $\hat{\mathbf{u}}$ is hereby the magnitude of the perturbation and ω_j is the frequency component for every frequency of the Fourier series. By inserting the residual of the flow solution and the perturbation of the grid in equation (4) with the stated assumptions and by rearranging the flow variable to the left side and the grid variables on the right side, the equation becomes:

$$\left(i\omega_j I + \frac{\partial \mathbf{R}}{\partial \mathbf{u}}\right)\hat{\mathbf{u}}_j = -\left(\frac{\partial \mathbf{R}}{\partial \mathbf{x}} + i\omega_j \frac{\partial \mathbf{R}}{\partial \dot{\mathbf{x}}}\right)\hat{\mathbf{x}}_j \tag{10}$$

In this equation $\partial\mathbf{R}/\partial\mathbf{u}$ defines the flux Jacobian, $\partial\mathbf{R}/\partial\mathbf{x}$ defines the grid node Jacobian and $\partial\mathbf{R}/\partial\dot{\mathbf{x}}$ defines the grid node velocity Jacobian. These first order partial derivatives can all be directly determined from the steady-state solution by the LFD solver. The complex component of the grid motion $\hat{\mathbf{x}}_j$ must be given for the solution of the equations. The remaining unknown variables are the complex-valued $\hat{\mathbf{u}}_j$, which are then solved in an iterative process. As a result, for each frequency ω_j and for a given grid motion $\hat{\mathbf{x}}_j$ the resulting behavior in the flow can be computed with the LFD solver by determing $\hat{\mathbf{u}}_j$. Since the grid motion $\hat{\mathbf{x}}_j$ is predefined by the user, the frequency response for different dynamic responses of the flap can be determined, as long as they are realistic and can be modeled in the deformation. Here, the dynamic response for the rotation of the flap is modeled. A detailed description of the derived equations and practicability of the LFD method is available in Thormann and Widhalm [6] and Da Ronch et al. [9]. Consequently, for

this process the LFD solver needs two components: First a well converged steady-state RANS solution and second a predefined periodic motion definition of small disturbances using a grid deformation.

In this application the LFD solver determines the lift coefficient derivative $\partial c_L/\partial \delta_\mathrm{f}$ of a flap in a defined flow condition. For a given frequency spectrum these derivatives are referred to as the frequency response $\hat{\mathbf{g}}$. The frequency response is a vector, which contains the respective magnitude and phase shift for all specified frequencies.
The deflection angle, at which the frequency response of the flap is defined, is intended to be variable. Therefore, the frequency response is computed at the mean deflection angle. In the LFD method of this work the mean deflection angle is defined as the time-averaged arithmetic mean value of the flap movement profile $\delta_\mathrm{f}(t)$:

$$\overline{\delta}_\mathrm{f} = \frac{1}{N}\sum_{n=0}^{N-1}\delta_\mathrm{f}(t_n) \tag{11}$$

In Fig. 3 the deformation of a grid for a plain flap with a mean deflection angle of 0° is shown. As a starting point in Fig.

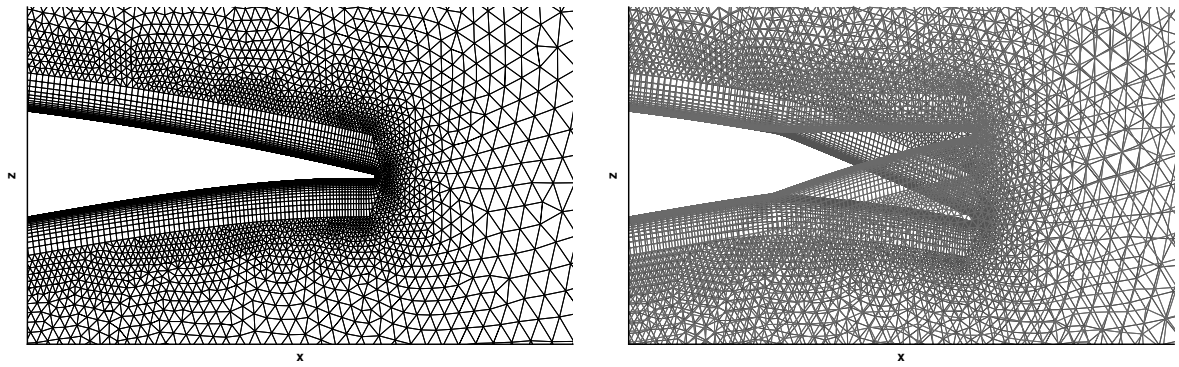

(a) grid for the steady-state solution at $\overline{\delta}_\mathrm{f} = 0°$

(b) grid deformation for $\delta_\mathrm{f} = \pm 10°$

Fig. 3 Illustration of the grid deformation for plain flap deflection angles of ±10°.

3 (a) the initial 2D grid for the trailing edge is depicted. For deriving $\hat{\mathbf{x}}$ in equation (10), the same number of grid nodes on initial and perturbed grid are required, therefore the perturbed grid is created by deformation of the initial grid. As an example two deformations, one with 10° downwards and one with 10° upwards flap deflection, are illustrated in Fig. 3 (b). The grid deformation is done by the TAU code using a radial basis function approach [20]. The center of rotation in this case is located at 80% of the chord. It is of importance that the flap deflections of ±10° in Fig. 3 are chosen for an improved illustration of the grid movement, in general they are too high for deriving $\hat{\mathbf{x}}$ in the LFD solver. The values of the two deflection should be close to the mean deflection angle to get a suitable derivative, therefore small deviations are preferred. For computing the frequency response, the LFD solver only needs deflections of ±0.1° at the mean deflection angle in order to define $\hat{\mathbf{x}}$. The implemented deformation itself allows deflections up to ±40° using the same initial grid, while still remaining a suitable grid for CFD computations. This ability is used for the URANS

computations, since it greatly increases their robustness and computation efficiency.

The flow solution is determined by RANS simulations and serves as the steady-state solution for the LFD solver. Derived from the residual in equation (7), it is required that the steady-state solution itself is converged close to machine accuracy. Here, the RANS solutions were converged to at least 10 orders of magnitude in density residual to achieve a sufficient accuracy.

Once the steady-state flow solution $\overline{\mathbf{u}}$ and grid deformation $\hat{\mathbf{x}}$ are determined, the LFD solver can calculate the real and imaginary part of the lift coefficient derivative $\partial c_L/\partial \delta_\mathrm{f}$ at the mean deflection angle for the first harmonic of a flap oscillating with a given frequency ω. The magnitude $r(\omega)$ of the dynamic response data for the first harmonic is defined as:

$$r(\omega) = \sqrt{\frac{\partial \hat{c_L}}{\partial \delta_\mathrm{f}}_{\mathrm{Re}}^{2} + \frac{\partial \hat{c_L}}{\partial \delta_\mathrm{f}}_{\mathrm{Im}}^{2}} \tag{12}$$

The related phase shift $\phi(\omega)$ is defined as:

$$\phi(\omega) = \arctan\left(\frac{\frac{\partial \hat{c_L}}{\partial \delta_\mathrm{f}}_{\mathrm{Im}}}{\frac{\partial \hat{c_L}}{\partial \delta_\mathrm{f}}_{\mathrm{Re}}}\right) \tag{13}$$

For a fixed flow condition and wing profile, using the computational efficiency of the LFD solver, the dynamic response data can now be computed for a chosen frequency spectrum. As a result, the frequency response $\hat{\mathbf{g}}$ is determined.

As shown in Fig. 2 (b), for a flap movement most components of the time frame occur in the low reduced frequency range of $k = 0 - 0.2$ at the given flight condition. For lowspeed flight conditions, frequency components of more than $k = 3$ only arise for flap rotation speeds of more than 100 °/s or especially sharp edged movement profiles. To obtain a convenient time interval and discretization for all possible input signals, its parametrization must be considered beforehand: The duration of the time interval should be long enough to allow for all perturbations to decay in the time period, since the application of the Fourier transform relies on a periodic signal. Therefore, the states of the flow at the beginning and at the end must be identical.

Additionally, the time resolution must be high enough to cover even fast deflection rates, so that the dynamic effects of the control surface are captured. Under these assumptions in this study the time interval duration has been set to 5 s. Discretized by $N = 200$ steps this yields a time step size of $\Delta t = 25$ ms or a sampling frequency of $f_s = 40$ Hz respectively. Following the Nyquist-Shannon sampling theorem, frequencies higher than $f = f_s/2 = 20$ Hz will be omitted during the process. For a higher resolution of frequencies the time period length of the flap movement profiles needs to be increased (see Eq. (1)).

Exemplarily, Fig. 4 shows a frequency response $\hat{\mathbf{g}}$ of a plain flap. The depicted frequency response was computed in a subsonic flow region on a transonic airfoil for a Mach number of Ma= 0.2 and covers viscous effects in the flow.

Although this is only an example of a frequency response, the qualitative characteristics of its dynamic behavior

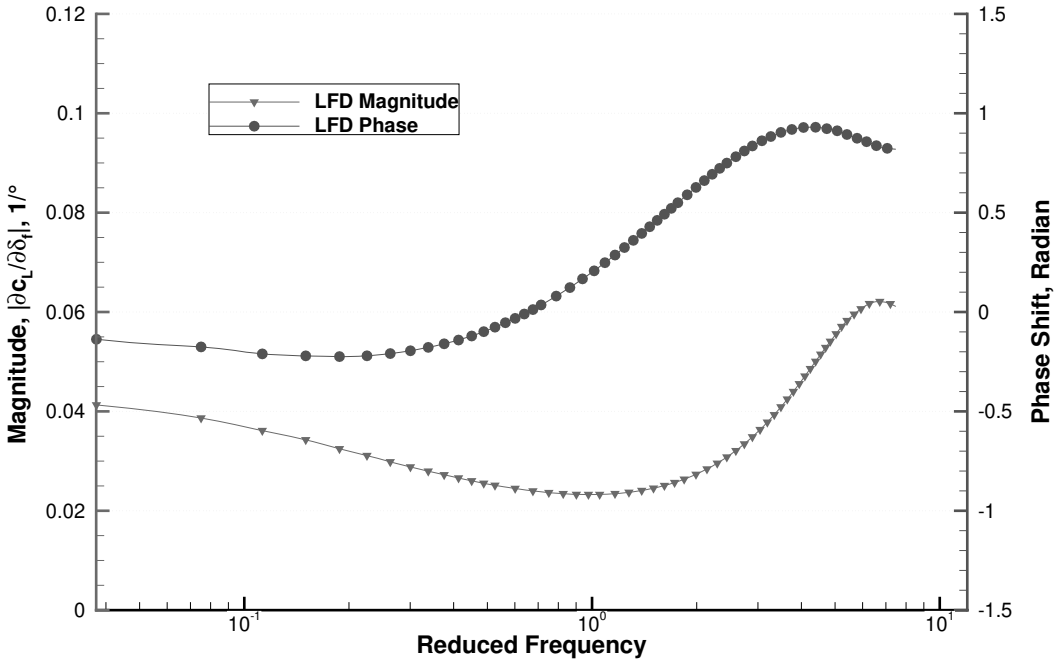

Fig. 4 Frequency response $\hat{g}$ of the plain flap under low speed flow conditions.

are representative for plain flaps in a subsonic flow region. First, the asymptote of the phase shift for the frequencies near zero appears to be also zero. At a frequency of $k = 0$ the dynamic response behavior for an infinitely slowly moving flap is described. Because there should be no unsteady effects in the flow for that case, the lift coefficient must always respond directly without the occurrence of any phase shift. Therefore, the asymptote of zero proves that the frequency response describes the correct phase shift of the plain flap for a frequency of $k = 0$. For higher frequencies the phase shift becomes negative up to a reduced frequency of $k = 0.6$, where the phase shift has a zero crossing. For higher reduced frequencies of $k > 0.6$ the phase shift becomes positive, which means the resulting response of the lift coefficient is preceding the flap movement. The maximum phase shift is reached near $k = 4$, where the delay is almost 16% or $\pi/3$ of the respective time period.

The asymptote of the magnitude for frequencies near zero is at $r \approx 0.043$ 1/°, which describes the efficiency of the flap on the lift coefficient for a static movement without any unsteady effects in the flow. The efficiency of the flap decreases up to a reduced frequency of $k = 1$, where its minimum at $r = 0.025$ 1/° is reached. Above frequencies of $k = 1$ the unsteady effects in the flow increase the magnitude of the flap efficiency up to a peak at $k \approx 6$, where the magnitude of the frequency response reaches the maximum of $r = 0.062$ 1/°. This shows that for a periodic movement in the higher frequency regions at $k > 1$ the unsteady effects in the flow lead to a preceding in the lift coefficient response and to an increasing impact on its magnitude.

D. Lift Coefficient from Flap movement

With a given flap movement profile in the frequency domain and a computed frequency response, the lift coefficient response of the control surface is determined by a superposition of magnitude and phase shift of the discrete frequencies. In this method the flap movement δ_f is the input, the lift coefficient response c_L is the output and the frequency response $\hat{\mathbf{g}}$ is considered as the gain of the system, which describes the dynamic response behavior between input and output in the frequency domain. The description given by the flap movement profile is purely geometrical and only provides information about the flap deflection angle regardless of the flight condition. The aerodynamic parameters of the flight condition such as Mach number, Reynolds number and angle of attack and the steady and unsteady response behavior of the control surface are all reflected in the frequency response $\hat{\mathbf{g}}$. For every discrete frequency ω, the sinusoidal input of the flap movement and the dynamic response behavior in the frequency response are merged by complex multiplication:

$$\hat{c}_L(i\omega) = \hat{\delta}_\mathrm{f}(i\omega) \cdot \hat{g}(i\omega) \tag{14}$$

Hence, the lift coefficient response in the frequency domain $\hat{c}_L(i\omega)$ is obtained, which is depicted in Fig. 5 (a) for the three generic flap movement profiles in Fig. 2.

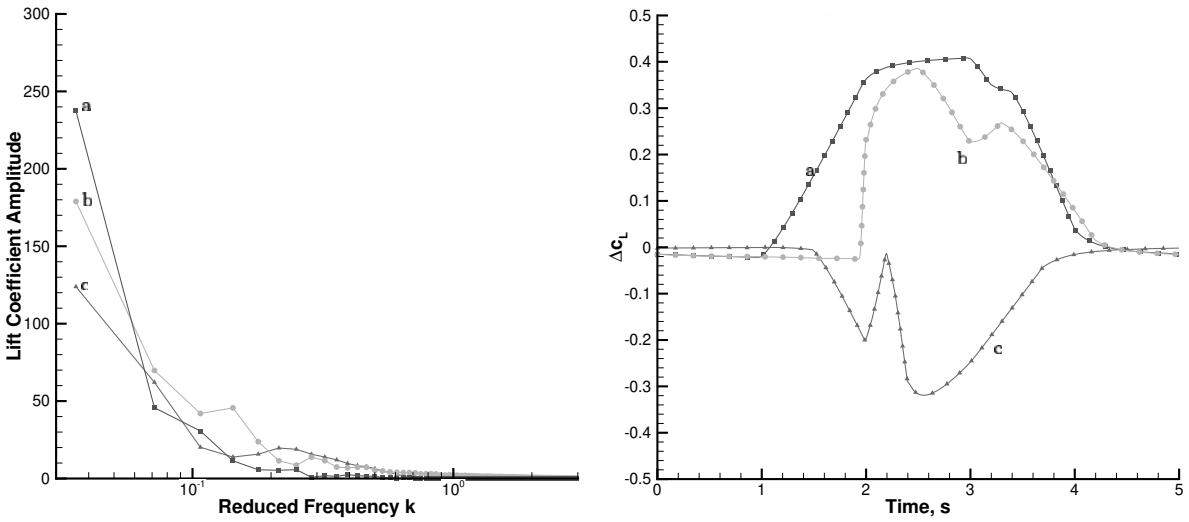

(a) frequency domain

(b) time domain

Fig. 5 Three lift coefficient response profiles in the frequency (a) and time domain (b).

By application of the inverse fast Fourier transformation (IFFT) the lift coefficient response of the frequency domain is shifted back into the time domain $c_L(t)$. Similar to equation (1) the transformation from the frequency components $\hat{c}_L(i\omega_j)$ into its time components $c_L(t_n)$ is defined by:

$$c_L(t_n) = \frac{1}{N}\sum_{j=0}^{N-1} \hat{c}_L(i\omega_j)e^{i\omega_j t_n}, \qquad t_n = n\Delta t, \qquad \omega_j = j\frac{2\pi}{N\Delta t}, \qquad n = 0, 1, ..., N-1 \tag{15}$$

The variable N is the number of frequency components and as well the total number of time steps for the lift coefficient response. The variable n is the index variable for every time step. Furthermore, the variable Δt is the interval between two time steps and $N\Delta t$ is the time period T for the response. For the three generic flap movement profiles the related lift coefficient response in the time domain $c_L(t)$ is illustrated in Fig. 5 (b). The lift coefficients are indicated relative to the lift for zero flap deflection on the airfoil.

IV. Process Chain of the Surrogate Model

In this section the surrogate model is introduced, which allows the computation of the aerodynamic lift coefficient response of a moving control surface within milliseconds. In the surrogate model the core LFD method is used to compute the lift generation in the frequency domain, with the difference in the way of calculating the frequency response. Here, frequency responses for the surrogate model are precomputed for different parameters to serve as samples in an interpolation space. In the online process the frequency response is then interpolated for a new data point.

A. Creation and Interpolation of sampling data using the SMARTy Toolbox

The surrogate model covers a parameter space spanned by five selected aerodynamic and geometric parameters. For the aerodynamic parameters Mach number *Ma*, Reynolds number *Re* and angle of attack α are chosen. In addition, as a geometric parameter for the plain flap, the relative flap chord size c_f/c is variable and for plain flap and Fowler flap the mean deflection angle $\overline{\delta}_f$ is available. Technically, the frequency response and thereby the lift coefficient can be evaluated for small sinusoidal excitations around the steady-state with 0° deflection angle. However, then the response is derived from the dynamic response behavior of the control surface at 0° deflection angle, which leads to decreasing precision for flap movements averaging outside of this deflection angle. Therefore, the mean deflection angle $\overline{\delta}_f$ is a variable parameter in the surrogate model, so that the dynamic response behavior at high positive and negative flap deflection angles is captured and available for lift coefficient prediction.

The frequency response $\hat{\mathbf{g}}$ only gives information about the lift response behavior relative to the mean deflection angle $\overline{\delta}_f$. To get the absolute c_L values, the steady lift coefficient $\overline{c}_L$ at the mean deflection angle needs to be added. Since the LFD solver requires a RANS solution at the mean deflection angle to compute $\hat{\mathbf{g}}$, the absolute $\overline{c}_L$ value at $\overline{\delta}_f$ is available. To get the absolute lift coefficient for the flap movement profile, the value of $\overline{c}_L$ replaces the zero-frequency component of equation (14):

$$c_L(i0) = \overline{c}_L \cdot N + i0 \tag{16}$$

The value $c_L(i0)$ is the complex frequency component of the lift coefficient response at the reduced frequency of k=0. As in equation (1), N is the number of points, in which the lift coefficient in the time domain is resolved. By replacing the zero-frequency element, the absolute lift coefficient value in the time domain is obtained. In order to get the absolute lift coefficient in the surrogate model for all flight conditions, the steady-state lift coefficients $\overline{c}_L$ from the RANS solution of the LFD solver for all samples are also recorded for the surrogate model. As a result, for every sample in the parameter space the lift coefficient $\overline{c}_L$ and the frequency response $\hat{\mathbf{g}}$ for the mean deflection angle $\overline{\delta}_\mathrm{f}$ is stored as sampling data in the surrogate model. The value $\overline{c}_L$ thereby represents the steady-state response and $\hat{\mathbf{g}}$ represents the dynamic response behavior of the flap for the mean deflection angle $\overline{\delta}_\mathrm{f}$.

The generation of the sampling parameters and the sampling data interpolation is performed by the DLR SMARTy toolbox. The acronym SMARTy stands for Surrogate Modeling for AeRo Data Toolbox and it is a software for the fast prediction of aerodynamic data based on high fidelity CFD [21][22]. For the generation of a surrogate model in the Offline section of the process around 100 samples are computed to cover up the parameter space. The sampling parameters for a uniform distribution of data points in the parameter space are provided using a deterministic Halton sequence [23]. In total the parameter space is spanned out in four dimensions: Ma, Re, α and $\overline{\delta}_\mathrm{f}$. The plain flap has an adjustable flap chord size c_f/c, therefore it has an additional fifth dimension. The interpolation of the scattered data in the SMARTy toolbox is done on a radial basis function interpolation model with a thin plate spline kernel[24].

B. Process chain structure

This section covers the entire process chain structure of the methodology for the fast prediction of aerodynamic response behavior of a control surface. In Fig. 6 a flowchart for the offline and online part of the surrogate model is depicted.

The first section of the flow chart covers the offline generation of sampling data for the subsequent usage in the online application part. As an input, range limits of the parameters are required to span out the parameter space for the surrogate model. Within these limits the SMARTy toolbox then creates sampling parameters for N number of samples. The aerodynamic parameters Ma, Re, and α are forwarded to the TAU solver. As a second input an undeformed grid of the flap system needs to be given. Using the geometric parameters c_f/c and δ_f, the grid deformation process provides the deformed grid x_n of the mean deflection angle $\overline{\delta}_\mathrm{f}$ to the TAU solver and the small perturbation deflections for deriving $\hat{x}$ to the LFD solver. The TAU solver then computes a well converged steady-state RANS solution to determine the time-averaged lift coefficient $\overline{c}_L$ and to provide a steady-state flow solution for the LFD solver. The LFD solver itself computes the frequency response $\hat{g}(i\omega)$ for every sample. These sampling data are used in the application section of the process chain structure.

Once the sampling data are generated, the online application process is working independently from the generation process. As an input the flap movement profile $\delta_\mathrm{f}(t)$ and the parameters Ma, Re, α, and c_f/c are required. For every given

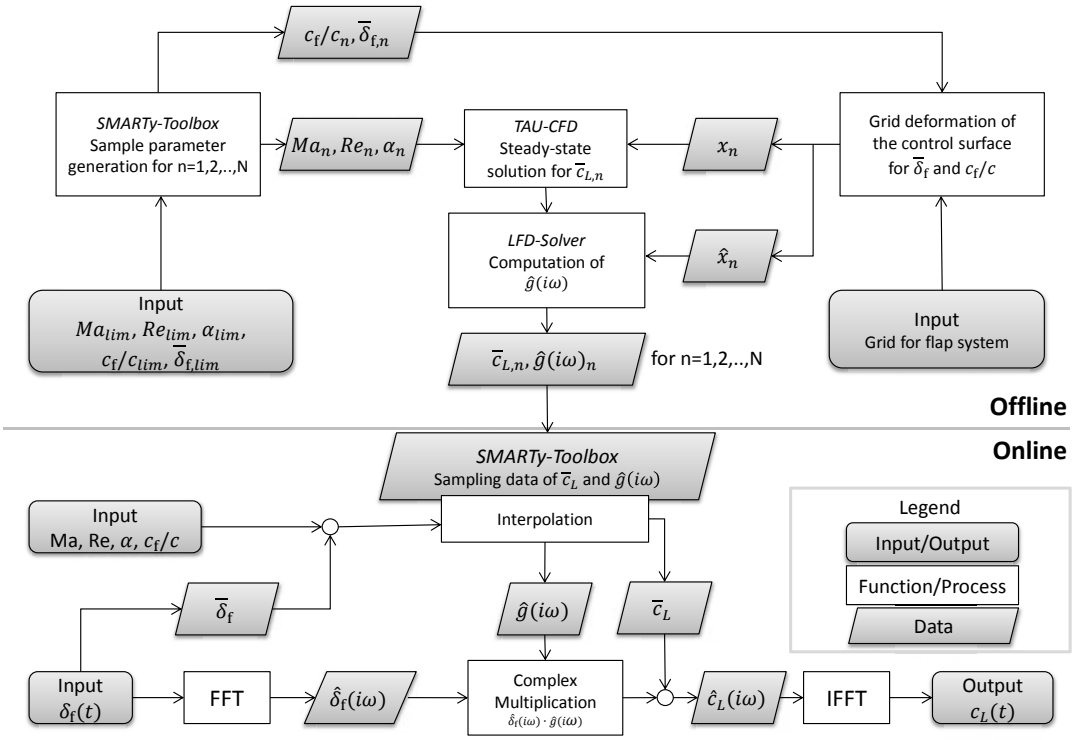

Fig. 6 Flowchart for building of the surrogate model offline and the online application.

set of inputs one solution for a lift coefficient response $c_L(t)$ is computed. The flap movement profile is transformed into the frequency domain using the FFT. The parameters Ma, Re, α, c_f/c, and the mean deflection angle $\overline{\delta}_f$ are forwarded to the SMARTy toolbox, which uses interpolation to get the appropriate frequency response $\hat{\mathbf{g}}$ and time-averaged lift coefficient $\overline{c}_L$ for this flight condition and flap configuration. The complex numbers $\delta_f(i\omega)$ and $\hat{g}(i\omega)$ are then multiplied in the frequency domain to get the lift coefficient response $c_L(i\omega)$ (see Eq. (14)). To get the absolute c_L values, the zeroth component of the lift coefficient response is replaced by $\overline{c}_L$ (see Eq. (16)). By using the IFFT the lift coefficient response is transformed back into the time domain $c_L(t)$, which is defined as the output of the entire process chain structure.

V. Results

In this section results of the surrogate model used on a 2D wing section of the XRF1 aircraft are shown. Results for a Fowler flap and a plain flap in low speed flow regions are presented. In addition, for the plain flap a surrogate model in transonic flow regions is displayed. URANS simulations are used for comparison in terms of accuracy and computation time.

A. Description of the XRF1 transonic airfoils

The computations for analysis and validation of the surrogate model were made on a 2D wing section on the XRF1 configuration, which is a typical configuration for a long-range wide-body aircraft provided by Airbus for research purposes. The Fowler flap is derived from the XRF1 in take-off configuration with an extended Fowler flap. The 2D section is located at approximately half of the wingspan. The flap movement is defined by a simple rotation of the Fowler flap close to its leading edge.

The second airfoil represents an aileron section and is taken on a 2D section on an outboard section of the wing. The implemented device for the second profile is a plain flap with an adjustable flap chord ratio c_f/c. For visualization in Fig. 1 exemplary transonic airfoils for both devices on a different geometry are shown. The following results refer to both devices, Fowler flap and plain flap.

B. Comparison of LFD-SM and URANS Results

The section details the comparison of the results for the surrogate model (SM) and URANS simulations. For validation of the surrogate model, results of the lift coefficient from time-dependent flap movements are compared for different flap types and flight conditions. For an improved clarity on the different computations the parameters for surrogate models for a lowspeed and a highspeed flight condition for the presented examples are listed in Table 1. Results of the entire process chain are referred to as LFD-SM in the following.

Leave-one-out tests were performed for testing of the required density of the samples in the parameter space of SM

Table 1 Parameters for the considered SMs and their specific cases.

Index	Description	Ma [-]	Re [-]	$\alpha[deg]$	$\overline{\delta}_f[deg]$	c_f/c [-]
SM 1	Fowler flap, lowspeed	$0.15-0.3$	$15-30\cdot10^6$	$-7-+15$	$-15-+0$	–
case 1a	takeoff	0.19	$21.5\cdot10^6$	8.0	$\overline{\delta}_f(t)$	–
case 1b	landing	0.18	$20\cdot10^6$	0.0	$\overline{\delta}_f(t)$	–
SM 2	plain flap, lowspeed	$0.15-0.3$	$15-30\cdot10^6$	$-4-+8$	$-10-+10$	$0.1-0.3$
case 2	-	0.2	$25\cdot10^6$	$2.0,\alpha$	$\overline{\delta}_f(t)$	0.2
SM 3	plain flap, highspeed	$0.7-0.75$	$35-40\cdot10^6$	$-1-+3$	$-2-+2$	$0.2-0.25$
case 3a	-	0.72	$36\cdot10^6$	2.0	$\overline{\delta}_f(t)$	0.22
case 3b	-	0.74	$38\cdot10^6$	0.5	$\overline{\delta}_f(t)$	0.24

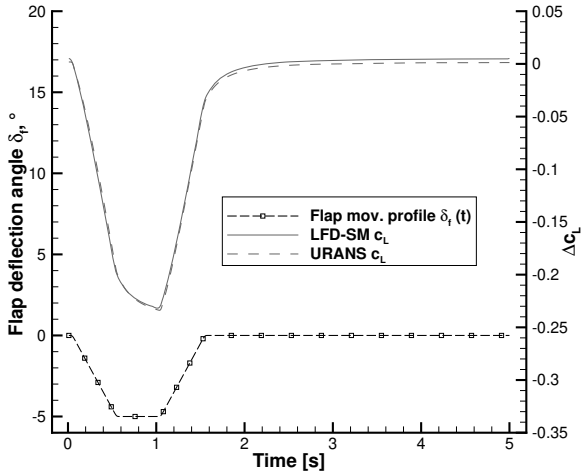

Fig. 7 Flap excitation and results from URANS and LFD-SM.

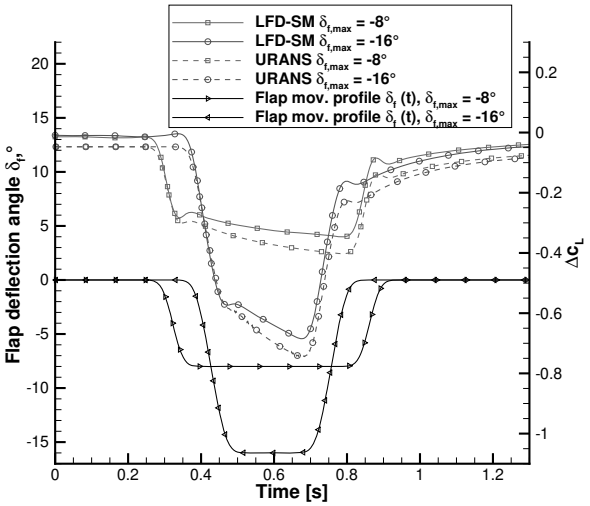

Fig. 8 Comparison of different flap excitations in full configuration.

2 (case 2). The steady-state lift coefficients showed a good agreement, most of the samples had a difference within ±0.01. In the bordering regions of the parameter space, the difference in the lift coefficient had maximum values of 0.03, which is, given the broad parameter space, still acceptable in terms of accuracy. The absolute difference between the norm of the actual frequency response $\hat{\mathbf{g}}$ and its reproduction $\hat{g}_{N-1}$, relative to the actual frequency response $\hat{\mathbf{g}}$, was acceptable in terms of accuracy of the interpolation. Only for parameters on the boundary of the parameter space the relative difference rose up to 0.1.

For convenience, the first results were obtained with the take-off configuration, as there are no shocks and the grid deformation is simple to implement. At take-off, slat and flap are both extended, the airfoil is pitched to a moderate angle of 8°, the flow is attached and there is margin in all parameters, where the flow stays attached. The flap movement profile follows a trapezoidal shape, where the flap angle is reduced by 5°. The movement profile is smoothed slightly, otherwise the infinite acceleration leads to distinct jumps in the history of the force coefficients. The settings used for this take-off configuration are listed in Table 1 (see case 1a).

As Fig. 7 shows, the results from the URANS solution and those determined from the computations of the LFD method show a very good agreement. Although the rotational speed of the flap is slow, unsteady effects are still visible in the lift coefficient response. The corresponding difference of URANS and LFD-SM prediction is less than $\Delta c_L = 0.003$ in the lift coefficient and acceptable regarding the accuracy. The deviating lift for zero excitation at the end of the signal can be traced back to the interpolation of the frequency response and the assumption of linear gradients in this area.

The results in Fig. 8 were obtained with the landing configuration at $\alpha = 0°$ (case 1b). Similar to the take-off computations a trapezoidal flap movement profile was used, but here with increased flap rotation speeds and deflection angles. In the case of $\Delta\delta_\mathrm{f} = -8°$ excitation the rotational speed is 136 °/s, with $\Delta\delta_\mathrm{f} = -16°$ the rotational speed peaks at

190 °/s. The duration of the flap excitation was calculated to yield an equal mean deflection angle for both profiles. As a result the interpolation of the steady lift should be the same for both cases and the frequency response is the only source for differences. Even in the steady-state lift coefficient both cases show a constant offset compared to the unsteady computations, which is originated in the too coarse resolution of samples in the surrogate model. Nevertheless, having the high rotational speed even higher harmonics appear when the flap comes to a halt, which show a good agreement with the LFD-SM results.

Furthermore, results of the surrogate model are shown on lowspeed and highspeed flow conditions of the plain flap. The geometry of the airfoil with the plain flap is actively deformed for the flap excitation and is suitable for the extensive analysis of the capabilities and characteristics of the surrogate model. The lift coefficient response for the flap movement profile from the surrogate model is compared to URANS computations for the same flight condition and control surface. The URANS computations were done using 1000 time steps for a time period of 5 seconds. The lift coefficients in the following figures are indicated relative to the lift generation for an angle of attack of 2° and 0° flap deflection angle. In Fig. 9 parameter studies for case 2 are presented.

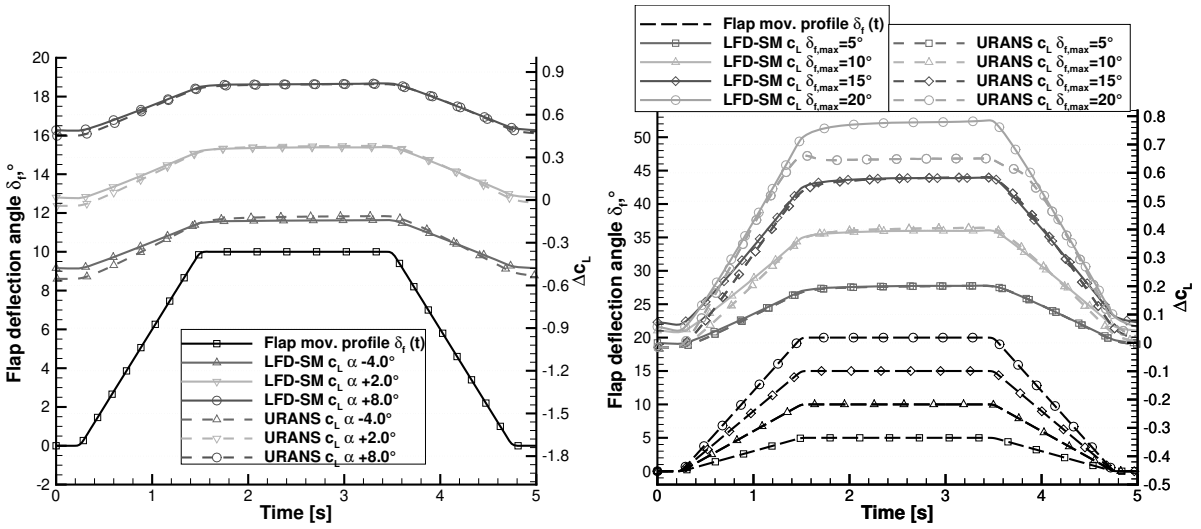

(a) angle of attack α variation

(b) maximum flap angle $\delta_{\mathrm{f,max}}$ variation

Fig. 9 Parameter studies for the surrogate model in comparison to URANS computations in case 2.

In Fig. 9 (a) the response behavior for the same flap movement up to $\Delta\delta_{\mathrm{f}}$ =10° is shown, while the angle of attack α is varied from -4° up to 8°. Both parts, the absolute and the dynamic part of the response from the surrogate model show a good agreement with the URANS computations. The dynamic part for $\alpha = -4°$ has a high maximum offset of $\Delta c_L = 0.07$, which is reasoned by its parameters being at the border of the parameter space. In Fig. 9 (b) the maximum flap deflection angle $\delta_{\mathrm{f,max}}$ in the flap movement profile is varied, while all other parameters are constant. For all deflection angles the computations show a good agreement in terms of accuracy. However, at a maximum angle of 20°

the URANS computations indicate flow separation at a deflection angle of 17° for this flight condition. Therefore, the prediction of the surrogate model differs and overshoots the lift coefficient value for the maximum lift coefficient. This case is an example to demonstrate the limits of the method, as the LFD method assumes the lift coefficient response to behave linear to the given input. In this case it can be seen that, by using the LFD method, the surrogate model is unable to predict arising nonlinear effects such as strong flow separation for an increasing flap deflection angle.

In Fig. 10 results of a highspeed surrogate model for two different flap movements profiles are shown. In Fig. 10 (a)

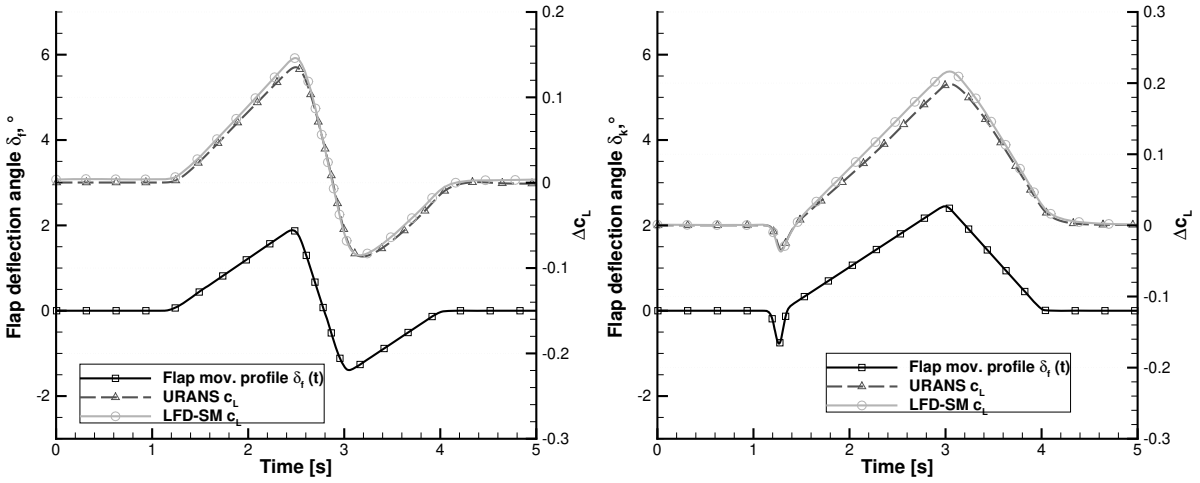

(a) Showcase 3a

(b) Showcase 3b

Fig. 10 Lift coefficient of a highspeed surrogate model for different flap movement profiles in comparison to URANS computations in case 3.

the lift response for a flap movement profile in the highspeed case 3a is depicted. Here, at Ma = 0.72 and an angle of attack of 2° a slow deflection in both directions of the flap is simulated. Similar in Fig. 10 (b) the lift response for a flap movement profile in the highspeed case 3b is presented, where at an angle of attack of 0.5° a high dynamic deflection at 1.2 seconds is applied and the mean deflection angle $\overline{\delta}_f$ for the movement is at 1°. Both cases show a good agreement of the lift coefficient accuracy in comparison to URANS computations. Even the dynamic aerodynamic effects at the turning points of the flap movement are caught sufficiently accurate by the surrogate model.

In Fig. 11 a special case for the capabilities of the LFD method is presented. In this figure all three lift coefficient responses were calculated for the same flight condition and flap movement appearance, with the difference in their time period length T. The flight condition is the same as in case 2, whereas the profile is varied for a time period T of $5s$, $0.5s$ and $0.1s$. By using this variation it is possible to compare the effects of quasi-steady aerodynamics with highly unsteady aerodynamics for equal flap excitation angles. For a time period of $5s$ the aerodynamics can be seen as quasi-steady, which means that due to the slow motion of the flap only minor unsteady aerodynamic effects arise in the

flow. In contrast, for the same flap movement in $0.1s$ highly unsteady aerodynamic effects influence the lift coefficient response. First, the c_L value at the beginning and the end of the time period are higher compared to the quasi-steady case. The LFD method assumes the input signal, in this example the flap movement, to be periodic and the response to achieve a transient state. Steady aerodynamics are unaffected for this condition, but for a periodic flap movement in a short time period of $0.1s$ unsteady aerodynamic effects of the previous period have influence on the next period. Furthermore, the fast flap deflection leads to additional positive offset of the lift coefficient of $\Delta c_L = 0.1$ for a positive rotation and a negative offset for a rotation back to 0° angle. These effects on the lift coefficient response are induced by unsteady aerodynamics in the flow. In comparison to URANS computations it can be seen that the solution of the LFD method covers all the characteristics in the response behavior and is able to predict unsteady aerodynamic effects with an acceptable accuracy.

In Table 2 the computation steps and total computational times for each method are listed. It is of importance that

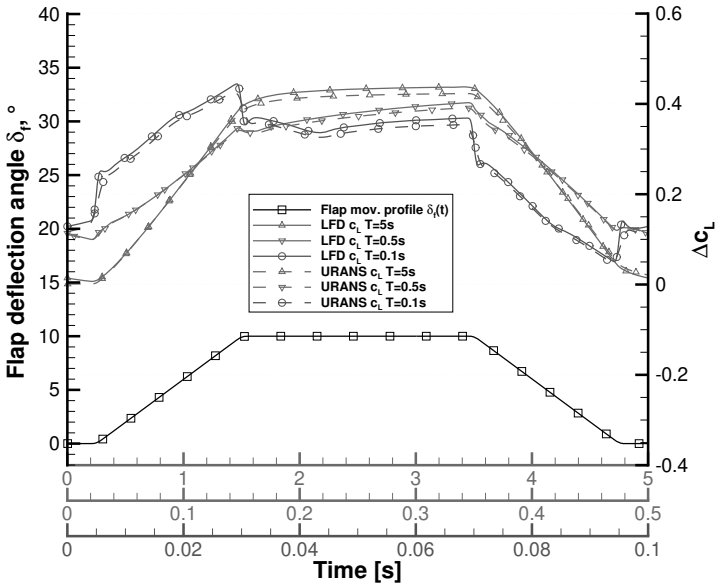

Fig. 11 Comparison of the same flap excitation for different time periods.

the computation times for the URANS equations and determination of the frequency response by the LFD solver are highly dependent on the numerical settings. Nevertheless, the shown results are configured for fast predictions, while maintaining a sufficient accuracy. The first method is the reference application by using the time-dependent URANS equation with a 1000 time steps in a time period of 5 seconds. The second method, labeled as LFD-only, describes the same process as in LFD-SM, but the frequency response $\hat{\mathbf{g}}$ is newly determined by the LFD solver for each specific case. For a number of 200 frequencies, which are required to discretize the frequency spectrum of this movement, the LFD-only method takes about 2 hours of time for computation and saves in total only one third of the URANS

computational time. However, for the surrogate model a number of 100 samples of frequency responses are computed to generate the sampling data in the parameter space. For every frequency response, with a number of 200 frequencies, it takes about 2 hours using the LFD solver, but the frequency responses for every sample can be computed independently and the generation for one parameter space is required only once. The online process determines the frequency response by mere interpolation of the given frequency response samples and in consequence avoids the expensive step of using the LFD solver. In a direct comparison it can be seen that the surrogate model (LFD-SM) computations achieve time reductions of more than 6 orders of magnitude in comparison to the URANS computations. This demonstrates the extreme advantage in terms of computation time by using the surrogate model for the prediction of aerodynamic response behaviors of control surfaces for arbitrary flap deflections.

Table 2 Quantitative comparison of the computational time for one flap movement profile with a time period of 5 seconds.

Method	Computation steps	Comput. time
URANS	Computation for every time step (here 1000 time steps , time step size $\Delta t = 0.005s$)	$\approx 3h$
LFD-only	FFT, $\hat{\mathbf{g}}$ for 200 frequencies with LFD solver ($\approx 2h$), IFFT	$\approx 2h$
LFD-SM	Offline: 100 samples of $\hat{\mathbf{g}}$ for 200 frequencies with LFD solver ($\approx 2h$), parallel	$\approx 100 \cdot 2h$
	Online: FFT, $\hat{\mathbf{g}}$ with interpolation ($\approx 2 \cdot 10^{-4}s$), Eq. 14, IFFT	$\approx 1.3 \cdot 10^{-3}s$

C. Limitations of the Methodology

The frequency response $\hat{\mathbf{g}}$ only quantifies the linear response behavior of the flap. It reflects no information on nonlinear responses in the flow due to high amplitudes of the movement of the flap, such as flow separation for high deflection angles or compression shocks in high speed applications. If nonlinear flow effects occur within the flap movement $\delta_f(t)$, the LFD method and thereby the surrogate model is unable to predict the response. It will then return the aerodynamic response, as if the aerodynamic response behavior of the flap would always remain linear.

In Fig. 12 an explicit case is shown, where the LFD method is unable to predict the correct lift coefficient response. For this analysis URANS computations on a plain flap for the flow condition case 2 (see Table 1) were evaluated. In all instances the flap had a sinusoidal excitation with a frequency of 0.1 Hz, while the amplitude for every instance differed from 2° to 40° of the deflection angle. Because the LFD method always requires the description of the flap movement and response to be periodic, the URANS computations were made in a time period of 60 seconds, so that a transient oscillation could be achieved. In Fig. 12 (a) the lift coefficient response of these instances are shown. It can be seen that up to a deflection angle of 16°, the lift coefficient has a sinusoidal shape. However, above that amplitude, especially for positive deflection angles, the flow separates and the flap is unable to increase the lift coefficient with a higher flap deflection angle. For analysis, for all instances in Fig. 12 (b) the lift coefficient responses were transferred into the frequency domain using the fast Fourier transform (Eq. (1)). Additionally, for improved comparability, every instance is

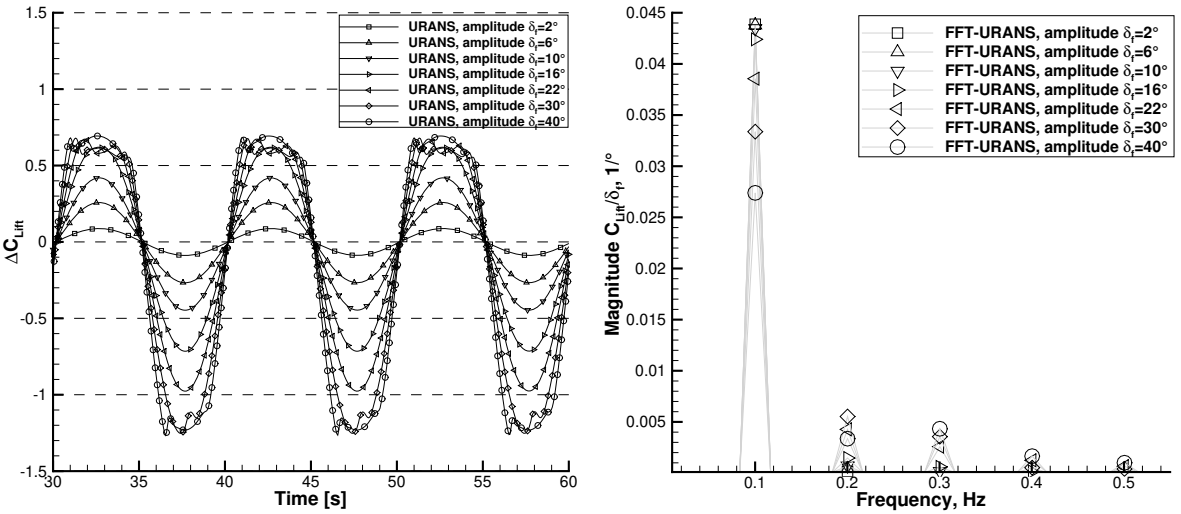

(a) time domain

(b) frequency domain

Fig. 12 Lift coefficient of URANS computations on a plain flap for sinusoidal excitations with $f = 0.1$ Hz and increasing amplitudes.

divided by its amplitude, therefore for every instance the relative lift generation per deflection angle in the frequency domain is shown. For every frequency the LFD solver only returns the response of the first harmonic. Here, for all instances with amplitudes below 16° the first harmonic at 0.1 Hz is dominant at 0.045 1/°, while there is a negligible magnitude on the higher harmonics. Since the first harmonic in the response is dominant for a sinusoidal input, the LFD method is able to predict its behavior accurately. Hence, this behavior is in contrast to the excitations of the flap with higher amplitudes. Above 16° amplitude the flow starts to separate and it can be seen that the relative impact of the first harmonic decreases. Furthermore, on the higher harmonics of 0.2 Hz and 0.3 Hz magnitudes of around $0.003 - 0.005$ 1/° arise. Because the LFD solver and thereby the frequency response $\hat{\mathbf{g}}$ only reflects the first harmonic in the response, it is by definition unable to predict the responses in the URANS computations for these instances due to the separation at higher amplitudes and the consequent shift of the response to higher harmonics.

Figure 13 compares the surface pressure distribution of URANS computations to the LFD predictions for different flap deflection amplitudes. The flap deflection thereby follows a sinusoidal curve with a frequency of 0.1 Hz for different amplitudes and the same mean deflection angle of $\overline{\delta}_\mathrm{f} = 0°$. In the figure the pressure distribution at the maximum positive flap deflection is depicted. It can be seen that for a small deflection of 6° the pressure distribution has a very good agreement with the URANS computations and only shows small deviations of 0.05 to 0.1 deviation of c_p at the leading edge and the kink of the flap. These effects grow stronger with increasing amplitudes up to 14° and especially the c_p distribution on the lower surface near the leading edge and the upper side of the kink start to diverge up to 0.15 c_p. For the leading edge this is induced by the movement of the stagnation point through the flap excitation, which

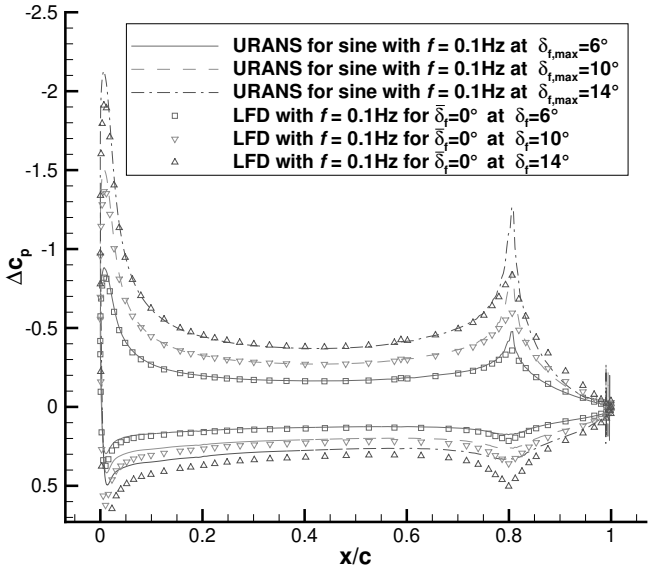

Fig. 13 Surface pressure distribution of URANS computations relative to $\delta_f = 0°$ on a plain flap for sinusoidal excitations with $f = 0.1$ Hz and increasing amplitudes.

leads to a nonlinear behavior of c_p between positive and negative flap deflection angles in this region. At the kink the forced deflection for a convex or concave deformation of the surface produces different shapes and therefore the pressure deviation magnitudes are not exactly matched by the LFD solver at this point. Nevertheless, due to integration of the values in the LFD method, these deviations counterbalance themselves and for this case the effects distort the lift coefficient only for deflection angles of $\delta_f > 16°$, as it can be seen in Fig. 12.

VI. Conclusion

This article introduces a surrogate model for the fast and accurate prediction of the aerodynamic response behavior for arbitrary control surface deflections. It is demonstrated that using a linear frequency domain method it is possible to simulate the aerodynamic response for arbitrary flap motions. The results in the lift prediction for the surrogate model show a good agreement in terms of accuracy with unsteady Reynolds-averaged Navier-Stokes computations. Once the surrogate model is generated, it is able to achieve computation time reductions of 6 orders of magnitude in comparison to URANS computations. The extremely fast predictions of the response behavior allow the application of the surrogate model for an extensive analysis of the efficiency of flap systems with respect to load alleviation. The wide parameter space, which is covered by the surrogate model, serves as a basis for the computation for different flight conditions and flap sizes. Furthermore, a geometric design study of the airfoil and the flap can be efficiently performed through the variation of the flap size parameter in the surrogate model.

By presenting results on two different flap systems, it is also demonstrated that the method is not restricted to a specific type of control surface. It is in fact applicable to further types of geometric alterations of the airfoil geometry, as long as they are feasible to be modeled in the grid deformation. Thus, also other types of control surfaces and the response behavior for different dynamic input variables aside from the flap deflection angle can be efficiently predicted with this methodology. Nevertheless, due to its nature the presented surrogate model is limited to dynamic flap motions in a linear response region. Nonlinear effects such as flow separation or shocks, which occur through high excitations of the flap movement, are not covered by this method.

For further studies on the usability of the LFD method, it is possible to use its characteristics as well for the linear response behavior to an angle of attack and a velocity variation. The surrogate model can thereby provide predictions for the control surface response and efficiency for an extensive gust analysis and load alleviation capabilities. Additionally, the process needs to be applied to a 3D control surface on a wing in order to prove its applicability and prediction quality for a more realistic use case.

References

[1] Xu, J., and Kroo, I., "Aircraft Design with Active Load Alleviation and Natural Laminar Flow," *Journal of Aircraft*, Vol. 51, No. 5, 2014, pp. 1532–1545. doi:https://doi.org/10.2514/1.C032402.

[2] Clark, W. S., and Hall, K. C., "A Time-Linearized Navier-Stokes Analyis of Stall Flutter," *Journal of Turbomachinery*, Vol. 122, No. 03, 2000, pp. 467–476. doi:https://doi.org/10.1115/1.1303073.

[3] Hall, K., Thomas, J., Ekici, K., and Voytovych, D., "Frequency Domain Techniques for Complex and Nonlinear Flows in Turbomachinery," *33rd AIAA Fluid Dynamics Conference and Exhibit*, 2003. doi:https://doi.org/10.2514/6.2003-3998.

[4] Dufour, G., Gourdain, N., and Sicot, F., "A Time-Domain Harmonic Balance Method for Rotor/Stator Interactions," *Journal of Turbomachinery*, Vol. 134, 2012. doi:https://doi.org/10.1115/1.4003210.

[5] Widhalm, M., Hübner, A. R., and Thormann, R., "Linear Frequency Domain Predictions of Dynamic Derivatives for the DLR F12 Wind Tunnel Model," *European Congress on Computational Methods in Applied Sciences and Engineering, ECCOMAS 2012*, Vienna, Austria, 2012.

[6] Thormann, R., and Widhalm, M., "Linear Frequency Domain Prediction of Dynamic Response Data for Viscous Transonic Flows," *AIAA Journal*, Vol. 51, No. 11, 2013, pp. 2540–2557. doi:https://doi.org/10.2514/1.J051896.

[7] Widhalm, M., and Thormann, R., "Efficient Evaluation of Dynamic Response Data with a Linearized Frequency Domain Solver at Transonic Separated Flow Conditions," *35th AIAA Applied Aerodynamics Conference*, 2017. doi:https://doi.org/10.2514/6.2017-3905.

[8] Ghoreyshi, M., and Cummings, R. M., "Unsteady Aerodynamic Modeling of Aircraft Control Surfaces by Indicial Response Methods," *AIAA Journal*, Vol. 52, No. 12, 2014, pp. 2683–2700. doi:https://doi.org/10.2514/1.J052946.

[9] Da Ronch, A., Ghoreyshi, M., J, B. K., Goertz, S., and Widhalm, M. e. a., "Linear Frequency Domain and Harmonic Balance Predictions of Dynamic Derivatives," *Journal of Aircraft*, Vol. 50, No. 3, 2013, pp. 694–707. doi:https://doi.org/10.2514/1.C031674.

[10] Bekemeyer, P., Thormann, R., and Timme, S., "Frequency-Domain Gust Response Simulation Using Computational Fluid Dynamics," *AIAA Journal*, Vol. 55, No. 7, 2017, pp. 2174–2185. doi:https://doi.org/10.2514/1.J055373.

[11] Bekemeyer, P., and Timme, S., "Reduced Order Gust Response Simulation using Computational Fluid Dynamics," *57th AIAA/ASCE/AHS/ASC Structures, Structural Dynamics, and Materials Conference*, 2016. doi:https://doi.org/10.2514/6.2016-1485.

[12] Bekemeyer, P., Thormann, R., and Timme, S., "Investigation into Gust Load Alleviation using Computational Fluid Dynamics," *International Forum on Aeroelasticity and Structural Dynamics, IFASD 2019*, 2019.

[13] Motta, V., and Quaranta, G., "Linear Reduced-Order Model for Unsteady Aerodynamics of an L-Shaped Gurney Flap," *Journal of Aircraft*, Vol. 52, No. 6, 2015, pp. 1887–1904. doi:https://doi.org/10.2514/1.C033099.

[14] Glaz, B., Liu, L., and Friedmann, P. P., "Reduced-Order Nonlinear Unsteady Aerodynamic Modeling Using a Surrogate-Based Recurrence Framework," *AIAA Journal*, Vol. 48, No. 10, 2010, pp. 2418–2429. doi:https://doi.org/10.2514/1.J050471.

[15] Seidler, R. B., Marten, S., Widhalm, M., and Wild, J., "Efficient Prediction of Aerodynamic Response Behavior for Control Surfaces using the Linear Frequency Domain," *AIAA Scitech 2019 Forum*, 2019. doi:https://doi.org/10.2514/6.2019-0427.

[16] Cooley, J. W., and Tukey, J. W., "An Algorithm for the Machine Calculation of Complex Fourier Series," *Mathematics of Computation*, Vol. 17, No. 90, 1965, pp. 297–301.

[17] Sears, W. R., "Some Aspects of Non-Stationary Airfoil Theory and Its Practical Application," *Journal of the Aeronautical Sciences*, Vol. 8, No. 3, 1941, pp. 104–108. doi:https://doi.org/10.2514/8.10655.

[18] Gerhold, T., "Overview of the Hybrid RANS Code TAU," *Notes on Numerical Fluid Mechanics and Multidisciplinary Design*, Vol. 89, 2005, pp. 81–92.

[19] Spalart, P., and Allmaras, S., "A One-equation Turbulence Model for Aerodynamic Flows," *30th Aerospace Sciences Meeting and Exhibit*, 1992. doi:https://doi.org/10.2514/6.1992-439.

[20] de Boer, A., van der Schoot, M., and Bijl, H., "Mesh deformation based on radial basis function interpolation," *Computers & Structures*, Vol. 85, No. 11, 2007, pp. 784 – 795. doi:https://doi.org/10.1016/j.compstruc.2007.01.013.

[21] Zimmermann, R., and Görtz, S., "Non Linear Reduced Order Models For Steady Aerodynamics," *Procedia Computer Science*, Vol. 1, No. 1, 2010, pp. 165–174. doi:https://doi.org/10.1016/j.procs.2010.04.019.

[22] Franz, T., Zimmermann, R., and Görtz, S., "Interpolation-based Reduced-order Modeling for Steady Transonic Flows via Manifold Learning," *International Journal of Computational Fluid Dynamics*, Vol. 28, No. 3-4, 2014, pp. 106–121. doi:https://doi.org/10.1080/10618562.2014.918695.

[23] Halton, J. H., "Algorithm 247: Radical-inverse Quasi-random Point Sequence," *Commun. ACM*, Vol. 7, No. 12, 1964, pp. 701–702. doi:https://doi.org/10.1145/355588.365104.

[24] L. Bookstein, F., "Principal warps: Thin-plate splines and the decomposition of deformations," *IEEE Transactions on Pattern Analysis and Machine Intelligence*, Vol. 16, 1992, pp. 567–585. doi:https://doi.org/10.1109/34.24792.